ChemPubSoc Europe
DOI: 10.1002/cctc.201500328
CHEMCATCHEM
Full Papers

Does the Surface Structure of Oxide Affect the Strong Metal–Support Interaction with Platinum? Platinum on Fe_3O_4(001) versus Fe_3O_4(111)

Ke Zhang, Shamil Shaikhutdinov,* and Hans-Joachim Freund[a]

We studied the structure and thermal stability of Pt deposited on a Fe_3O_4(001) thin film to make a comparison with the Pt/Fe_3O_4(111) system that shows a strong metal–support interaction (SMSI) through encapsulation. Pt adatoms interact strongly with the $(\sqrt{2}\times\sqrt{2})R45^{\circ}$-reconstructed Fe_3O_4(001) surface and adsorb monoatomically on the "narrow" sites. Metal sintering sets in only above 700 K to result in cuboid Pt nanoparticles exposing primarily (100) and (110) facets. Concomitantly, CO adsorption on Pt is fully suppressed as a result of the SMSI. The results provided strong evidence that the Pt nanoparticles on Fe_3O_4(001) are encapsulated by an FeO(111) layer in the same manner as observed for hemispherical Pt particles on Fe_3O_4(111). The comparison suggests that the SMSI effect through encapsulation is insensitive to the surface structure of the oxide, although the latter strongly affects the particle morphology.

Introduction

The strong metal–support interaction (SMSI),[1] often observed for metal particles supported on reducible oxides, is discussed mostly in terms of the encapsulation of the metal by the oxide.[2] Although the encapsulation may, to some extent, be rationalized on thermodynamic grounds using surface energy considerations, an atomic description of how a metal particle becomes covered by an oxide is still missing. Another interesting yet poorly studied issue is whether the SMSI effects are structure sensitive, that is, dependent on the surface structure of the oxide support. Indeed, the interaction depends primarily on the adhesion energy between the metal and the oxide, which is envisioned to depend on the interface structure. To gain a fundamental understanding of the SMSI effects, model studies are performed, in which metal nanoparticles are deposited in a controllable manner on well-defined oxide surfaces in the form of single crystals or thin films.[3] In particular, previous studies on Pd/TiO_2(110)[4] and Pt/Fe_3O_4(111)[5] indicated that the encapsulation proceeds through mass transport along the surface rather than through the metal particle.

With respect to iron oxides as a typical reducible oxide support, model studies focused primarily on the Fe_3O_4(111) surface.[6] In particular, our own studies on metal (Au, Pd, Pt) deposited on Fe_3O_4(111) thin films showed the formation of hemispherical nanoparticles that expose (111) top facets.[3b,7] To date, only Pt was found to exhibit the SMSI effect through encapsulation by a FeO(111) single layer.[5,8] Recently, more work has been directed toward the Fe_3O_4(001) surface following expectations of a large difference in reactivity compared to the (111) surface (see, for example, Ref. [9]).

High-resolution STM studies of Au,[10] Pd,[11] and Ag[12] on the well-defined $(\sqrt{2}\times\sqrt{2})R45^{\circ}$-reconstructed surfaces of Fe_3O_4(001) showed a strong interaction and remarkable thermal stability of the metal adatoms. High-energy electron diffraction, TEM, and AFM studies of Pt, Au, and Ag films of a few nanometers in thickness on a Fe_3O_4(001) substrate revealed certain epitaxial relationships between the metal and iron oxide depending both on the nature of the metals and the deposition temperature (470–1000 K).[13] The authors concluded that among the metals studied, Pt is the metal for which the adhesion energy to Fe_3O_4 is the highest, although it has the largest mismatch between the lattice constants compared to Ag and Au. (However, the surface termination of the Fe_3O_4(001) films grown on MgO(001) used in this study was not determined).

Magnetite Fe_3O_4 has an inverse spinel structure. It is generally accepted that the Fe_3O_4(111) surface is terminated by Fe atoms coordinated tetrahedrally over the close-packed oxygen layer (Figure 1 a), although it depends critically on the preparation conditions.[6d,14] In the $<001>$ direction, the so-called "B-layer" termination, which consists of mixed Fe and O atoms coordinated octahedrally, seems to be the most stable over a broad range of oxygen pressures as predicted by DFT (Figure 1 b).[15] Although it is well documented that the Fe_3O_4(001) surface exhibits a $(\sqrt{2}\times\sqrt{2})R45^{\circ}$ reconstruction, its atomic structure remains controversial. Recently, based on quantitative low-energy electron diffraction (LEED) and STM studies combined with DFT calculations, the reconstruction has been ra-

---

[a] K. Zhang, Dr. S. Shaikhutdinov, Prof. Dr. H.-J. Freund
Abteilung Chemische Physik
Fritz-Haber-Institut der Max-Planck-Gesellschaft
Faradayweg 4-6, 14195 Berlin (Germany)
E-mail: shaikhutdinov@fhi-berlin.mpg.de

Supporting Information for this article is available on the WWW under http://dx.doi.org/10.1002/cctc.201500328.

This publication is part of a Special Issue on Advanced Microscopy and Spectroscopy for Catalysis. Once the full issue has been assembled, a link to its Table of Contents will appear here.

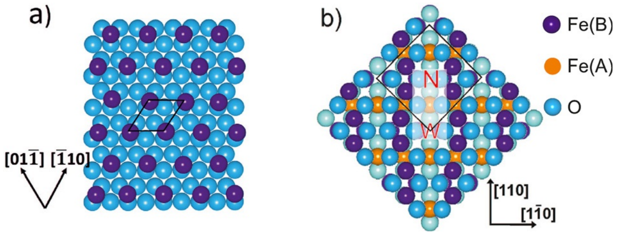

Figure 1. Top views and the units cells of a) the $Fe_3O_4(111)$ and b) the $(\sqrt{2}\times\sqrt{2})R45^\circ$-reconstructed $Fe_3O_4(001)$ surfaces. The wide (W) and narrow (N) sites in the $(\sqrt{2}\times\sqrt{2})R45^\circ$-$Fe_3O_4(001)$ unit cell are indicated.

tionalized in terms of an ordered array of subsurface Fe vacancies and interstitials.[16]

In this work, we address the nucleation, growth, and thermal stability of Pt particles on the $(\sqrt{2}\times\sqrt{2})R45^\circ$-$Fe_3O_4(001)$ surface and compare the results with those obtained previously in our laboratories for the Pt/$Fe_3O_4(111)$ system, which exhibits a classical SMSI effect through encapsulation as demonstrated clearly by STM and CO adsorption studies. In contrast to the hemispherical particles obtained for Pt on $Fe_3O_4(111)$, the Pt nanoparticles on $Fe_3O_4(001)$ shown here assume a cuboid shape upon annealing at high temperatures. Nonetheless, the Pt particles become encapsulated by an iron oxide overlayer, which is an FeO(111) monolayer in nature, that is, in the same manner as on an $Fe_3O_4(111)$ support. The results shed more light on the structure sensitivity of the SMSI effects on Pt-based catalysts.

Results and Discussion

As reported in our previous paper,[17] pristine $Fe_3O_4(001)$ thin films expose wide, flat terraces with few screw dislocations. A high-resolution STM image that shows the atomic rows running in the $<110>$ direction characteristic for the $(\sqrt{2}\times\sqrt{2})R45^\circ$ reconstruction is shown in Figure 2a. In addition, defects imaged either as weak depressions or protrusions ≈ 1 Å in depth (height) are observed frequently (see inset in Figure 2a). Both features are located over the protruding rows that correspond to the octahedral Fe atoms in the topmost layer[10a, 11, 18] (Figure 1b). Following Parkinson and co-workers,[10a] we assign adspecies to adventitious hydroxyl groups formed by the reaction with residual gases in our ultra-high vacuum (UHV) chamber. Accordingly, the depressions could tentatively be attributed to Fe vacancies in the topmost layer.

An STM image after the deposition of 0.15 monolayers (ML) of Pt at 300 K is shown in Figure 2b (1 ML of Pt corresponds to one Pt atom per $(\sqrt{2}\times\sqrt{2})R45^\circ$ surface unit cell, that is, 1.4×10^{-14} at cm^{-2}). Besides the weak OH protrusions that remain at the surface, two other types of protrusions are observed that must, therefore, be attributed to Pt. Most of the additional protrusions are ≈ 2.5 Å in height and are located between the Fe rows. These are assigned to single Pt atoms in the same manner as for Pd, Au, and Ag.[10a, 11, 12] Again, the registry analysis (Figure 2c) reveals that the Pt atoms occupy the so-called "narrow" sites on the $(\sqrt{2}\times\sqrt{2})R45^\circ$-reconstructed $Fe_3O_4(001)$ surface.

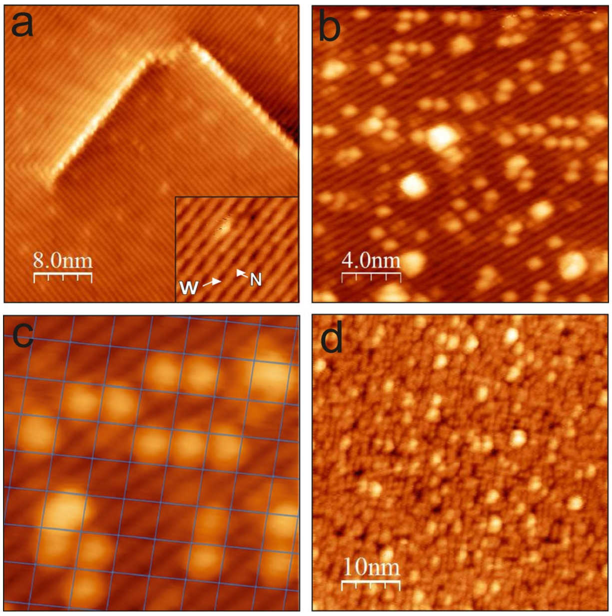

Figure 2. STM images of a) a clean $Fe_3O_4(001)$ film and b, c) after the deposition of 0.15 ML and d) 1 ML Pt at 300 K. Wide (W) and narrow (N) adsorption sites (see Figure 1b) within the $(\sqrt{2}\times\sqrt{2})R45^\circ$-$Fe_3O_4(001)$ unit cell are indicated in the inset in panel a. In panel c, the lines join the wide sites, therefore, the Pt adatoms occupy the narrow sites. (Tunneling conditions: a) bias −1 V, current 0.5 nA; b, c) −1 V, 0.7 nA; d) −1.5 V, 1 nA).

Additionally, a few larger protrusions of ≈ 6 Å in height and ≈ 15 Å in lateral size are observed, which are assigned to Pt clusters. The Pt adatoms and clusters are distributed randomly on the entire oxide surface and show no preferential nucleation on step edges and screw dislocations. This implies the relatively strong interaction of the Pt atoms with the $(\sqrt{2}\times\sqrt{2})R45^\circ$-$Fe_3O_4(001)$ surface that results in limited surface diffusion that, in turn, prevents Pt agglomeration into the larger clusters. The formation of Pt clusters in our experiments may also result from the adsorption of residual gases (such as CO) as shown previously for Pd adatoms.[11]

Basically, such a nucleation–growth mode remains at increasing Pt coverage up to 1 ML, upon which the surface is mostly covered by Pt adatoms, although the density of 3D nanoparticles apparently increases (Figure 2d). Similar behavior was reported previously for Ag adatoms.[12] The higher density of nanoparticles observed here for Pt compared to Ag may be explained by the stronger interaction of Pt adatoms with residual gas molecules, which, in turn, weaken the Pt bonds to the support. Indeed, Au adatoms, as presumably more weakly bound species, showed sintering at considerably lower coverages.[10a]

In the next set of experiments, we examined the thermal stability of the Pt deposits by stepwise annealing in UHV at elevated temperatures. A series of STM images obtained for 1 ML Pt/$Fe_3O_4(001)$ is shown in Figure 3. Compared to the "as-deposited" sample (Figure 2d), UHV-annealing at 500 K for 10 min does not cause considerable morphological changes (Figure 3a), although the density of clusters increases. Metal sintering only becomes substantial after annealing at 700 K (Figure 3b). The Pt nanoparticles can clearly be recognized and

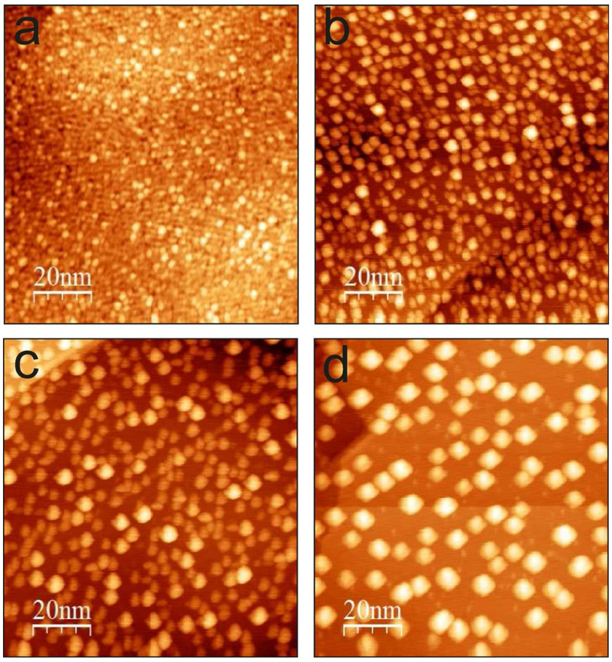

Figure 3. STM images of 1 ML Pt/$Fe_3O_4(001)$ annealed stepwise at a) 500 K, b) 700 K, c) 850 K, and d) 1000 K. (Tunneling conditions: bias −2 V, current a, b) 0.7 nA; c, d) −2 V, 1 nA).

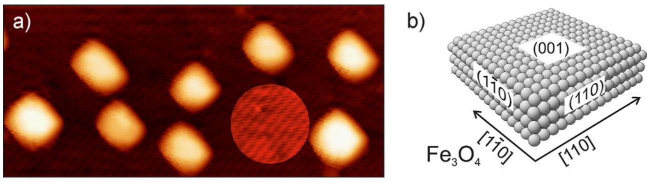

Figure 4. a) STM image of 1 ML Pt/$Fe_3O_4(001)$ annealed at 1000 K. The atomic rows of the support are highlighted in the circle to show the orientation of the particles with respect to the support. (Tunneling bias −1.5 V, and current 1 nA). b) Schematic representation of the cuboid Pt particles.

they grow both laterally and in height at the expense of monoatomic species. Further sintering, presumably by Ostwald ripening, proceeds upon heating to 850 K (Figure 3c). Ultimately, after annealing at 1000 K, Pt nanoparticles with a cuboid shape dominate the surface (Figure 3d).

The high-resolution STM image in Figure 4a reveals that the edges of the Pt particles are oriented along the Fe rows on the surrounding $(\sqrt{2}\times\sqrt{2})R45^\circ$-reconstructed surface of $Fe_3O_4(001)$. Solely based on these STM images, one can envision that Pt grows in the (001) orientation parallel to the (001) plane of Fe_3O_4, similar to the epitaxial relationships reported in Ref. [13], although these were observed on 2–5 nm thick Pt films grown on $Fe_3O_4(001)$ at high temperatures. Our previous LEED results for the growth of $Fe_3O_4(001)$ films on a Pt(001) substrate showed that lattice vectors of Pt(001) are oriented along the lattice vectors of $Fe_3O_4(001)$-(1×1).[17] It is, therefore, plausible that the same mutual orientation holds true for the inverse interface, that is, Pt on an $Fe_3O_4(001)$ substrate. This suggests that the atomic rows on Pt(001) facets run along the Fe rows on the $(\sqrt{2}\times\sqrt{2})R45^\circ$-reconstructed $Fe_3O_4(001)$ surface (Figure 1b). Based on this and electron microscopy diffraction patterns reported in Ref. [13], we can envision a truncated Pt cuboid particle as shown schematically in Figure 4b.

Similar annealing experiments performed on 1.5 and 4 ML Pt samples revealed essentially the same behavior: Sintering sets in at around 700 K with the progressive formation of the well-shaped Pt nanoparticles at elevated temperatures. For comparison, the morphologies of samples annealed to 1000 K are shown in Figure 5. Again, all annealed particles ultimately showed the cuboid shape. The annealing time needed to reach such a shape is relatively long, that is, around 30 min. The annealing of 1.5 ML Pt sample for 10 min resulted in a mixture of hexagonal and rectangular top facets (Figure 5b). The latter dominate the surface only after further annealing for 30 min (Figure 5c). For the highest Pt coverage studied here (4 ML), some template effects can be seen in the image shown in Figure 5d, as the cuboid Pt particles form quasiordered arrays along the crystallographic directions of the support. Interestingly, with increasing Pt coverage, the lateral size of the annealed particles, on average, remains the same, and only the particle density and heights increase.

To address the SMSI effects on high-temperature annealing, we performed temperature-programmed desorption (TPD) experiments using CO as a probe molecule to titrate the Pt surface as the iron oxide support does not adsorb CO at 300 K. CO-TPD plots obtained on the 1.5 ML Pt/$Fe_3O_4(001)$ surface annealed stepwise at the specified temperatures are shown in Figure 6a. Structural characterization after each annealing step was performed by STM and LEED.

The "as-deposited" Pt/$Fe_3O_4(001)$ surface showed a broad desorption signal between 300 and 520 K with a maximum at 450 K, which falls into the range observed for single-crystal Pt surfaces.[19] However, CO-induced sintering of the Pt adatoms,

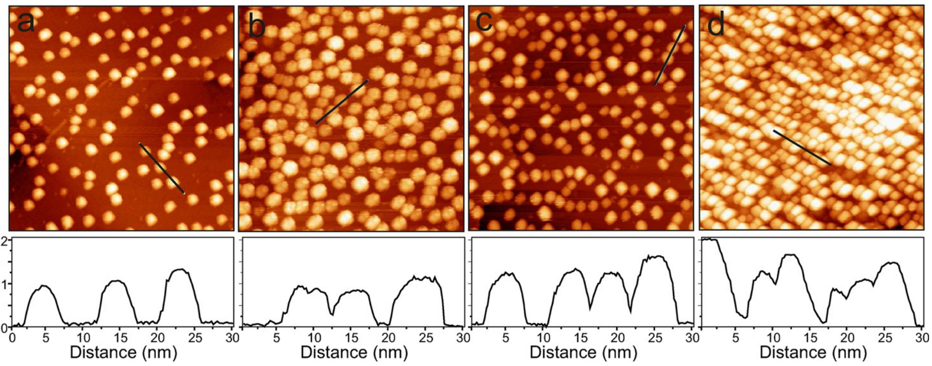

Figure 5. STM images and corresponding profile lines of the Pt/$Fe_3O_4(001)$ samples, all annealed at 1000 K. a) Pt coverage is 1 ML, and the annealing time is 30 min; b) 1.5 ML, 10 min; c) 1.5 ML, 40 min; d) 4 ML, 30 min. All image sizes are 100 nm × 100 nm. Tunneling conditions: a) bias −2 V, current 1 nA; b–d) −1.5 V, 1 nA.

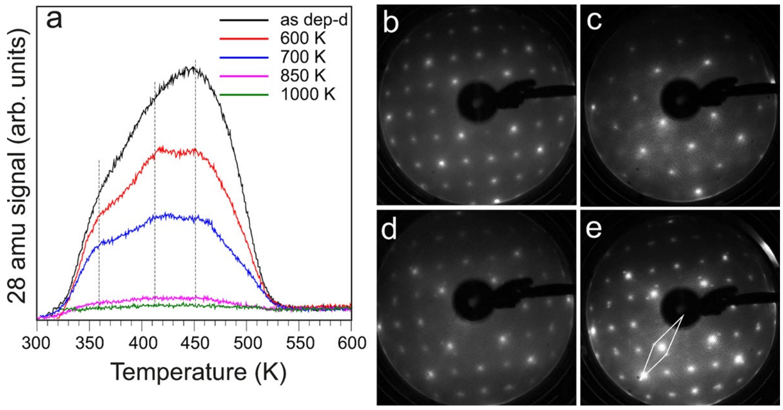

Figure 6. a) TPD spectra of 20 L CO adsorbed at 300 K on 1.5 ML Pt/Fe_3O_4(001) as deposited at 300 K and then UHV-annealed to the indicated temperature. The heating rate is 2 $K\,s^{-1}$. LEED patterns (at 95 eV) of b) the pristine ($\sqrt{2}\times\sqrt{2}$)R45°-Fe_3O_4(001) surface, c) after deposition 1.5 ML of Pt at 300 K, and d) after subsequent UHV-annealing to 850 K for 10 min and e) 1000 K for 30 min, respectively. The additional spots are developed, which are assigned to the FeO(111)/Pt(001)-c(2×10) structure as marked in panel e.

as observed previously for Pd/Fe_3O_4(001),[11] might also affect the first TPD plot. Annealing at 600 K slightly (by ≈15%) reduces the CO uptake, and several desorption features at 360, 420, and 450 K can be resolved. These features remain after annealing at 700 K, which further reduces the CO uptake. The latter decreases to almost zero upon annealing to 850 K, although Pt particles did not show considerable sintering (Figure S1), thus providing direct evidence that the Pt particles exhibit the SMSI effect at elevated temperatures most likely through encapsulation. Indeed, the formation of Pt-Fe alloys as another option to explain the decreased CO uptake would manifest itself as a prominent desorption signal at around 300 K,[20] which is not the case here. Ultimately, annealing at 1000 K suppresses CO adsorption totally and it is accompanied by the reshaping of the Pt particles.

LEED patterns of the same Pt/Fe_3O_4(001) surfaces recorded before the TPD runs are shown in Figure 6b–d. Additional diffraction spots (marked in Figure 6e) appear upon annealing that were absent on the pristine Fe_3O_4(001) film annealed at the same temperature (1000 K) before Pt deposition. These spots first develop upon heating to 850 K and become more intense and sharper by annealing at 1000 K. The corresponding surface structure is virtually identical to that observed for an ultrathin iron oxide film grown on a Pt(100) single crystal and assigned to an FeO(111)/Pt(100)-c(2×10) (and/or -(2×9)) coincidence structure.[21] Bearing in mind the cuboid morphology of the annealed Pt nanoparticles, which preferentially expose the top (100) facets (Figure 4b), the LEED observation of the FeO(111)/Pt(100) interface can readily be explained by the encapsulation of the Pt particles by an FeO(111) layer. One could argue, however, that the new ordered structure arises from the interface underneath rather than on top of a Pt particle, although the spots seem to be too bright to make the former assignment.

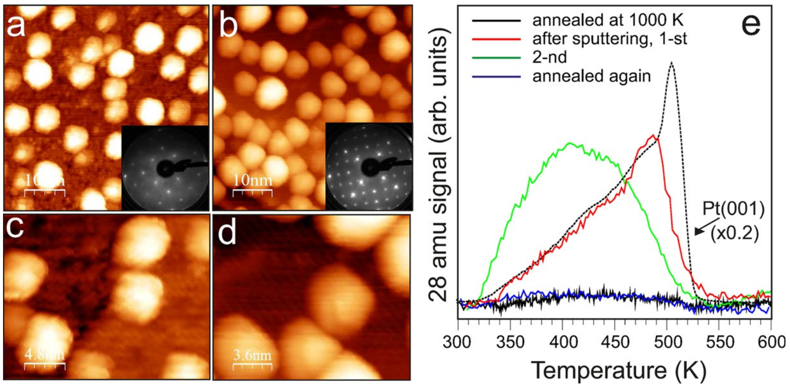

Figure 7. a–d) STM images and corresponding LEED patterns (at 95 eV in insets) of 1.5 ML Pt/Fe_3O_4(001) annealed at 1000 K for 30 min and then a, c) Ar^+ ion sputtered at 300 K and b, d) reannealed at 1000 K for 10 min. (Tunneling conditions for all images are bias −1.5 V, and current 1 nA). e) TPD plot of 20 L CO adsorbed at 300 K on the same samples as indicated. The heating rate is 2 $K\,s^{-1}$. The plot of the clean, hex-reconstructed Pt(001) surface, measured before growth of the Fe_3O_4(001) film is shown as a dashed line for comparison.

To shed more light on this issue, we have performed sputtering experiments as follows. The 1.5 ML Pt sample annealed to 1000 K was subjected to a mild Ar^+-ion bombardment (500 eV, ≈1 $\mu A\,cm^{-2}$, 45° incidence, for 10 s) at room temperature. Certainly, this treatment caused some surface roughening as judged by STM (Figure 7a). However, the atomic rows of the ($\sqrt{2}\times\sqrt{2}$)R45°-reconstructed Fe_3O_4(001) between the particles are still visible (Figure 7c), thus indicating that ion bombardment under our conditions does not cause severe sputtering but creates surface defects. However, the FeO(111)/Pt(100) diffraction spots fully disappear (inset in Figure 7a). Moreover, CO starts to adsorb on the sputtered surface as observed by TPD (Figure 7e), which indicates that the ion sputtering removed the encapsulating layer and exposed the Pt surface.

Interestingly, the first CO-TPD plot revealed a prominent peak at ≈500 K, which shows similarities to the plot measured on the clean hex-Pt(001) surface. It is tempting to assign this feature to the top (100) facets of the Pt particles opened upon ion sputtering of the encapsulated layer. However, such a TPD profile can also be associated with highly stepped Pt surfaces[19] and, more generally, to the low-coordinate Pt atoms formed on the Pt particles upon sputtering of the Pt surface beyond the encapsulating layer. Indeed, the second CO-TPD run already showed a broad signal similar to that measured on "as-prepared" Pt particles (Figure 6a). Reannealing of the sample at 1000 K for 10 min, in essence, recovers the initial characteristics of the sample before treatment: the FeO(111)/Pt(100) diffraction spots reappear and the CO uptake decreases back to zero.

Therefore, the above-presented LEED, STM, and TPD results provide strong evidence that Pt nanoparticles undergo the SMSI effect by encapsulation by an iron oxide layer, which is an FeO(111) monolayer in nature. Unfortunately, atomic resolution of the Pt particles could not be achieved with our microscope (basically, because of their small size), which would otherwise allow us to determine the atomic structure of the Pt top facets more precisely.

Nonetheless, we are now in the position to compare the structural properties of Pt/Fe_3O_4(001) and Pt/Fe_3O_4(111) systems[3b,c,8] using thin-film supports grown on Pt(100) and Pt(111) substrates, respectively. On both the (001) and (111) magnetite surfaces, Pt shows no preferential nucleation on defects and appears to be dispersed uniformly across the entire surface. Pt on the ($\sqrt{2}\times\sqrt{2}$)R45°-Fe_3O_4(001) surface adsorbs monoatomically, even at 300 K, and occupies the "narrow" sites. On Fe_3O_4(111), the adsorption sites for Pt were not yet determined as STM imaging at low Pt coverages is obscured by the presence of poorly defined adsorbate-like species.[14a,22] As DFT predicts the strong adsorption of Pt on Fe_3O_4(111) (i.e., ≈2.2 eV on the Fe-terminated surface),[23] one could envision monoatomic Pt adsorption on Fe_3O_4(111) as well. Indeed, STM images of Pt/Fe_3O_4(111) at sub-monolayer coverages revealed a high density of small islands, which are only ≈2 Å in height and correspond to a single Pt layer.[3c] At increasing coverages, the monolayer islands coalesce and form an extended, irregularly shaped network, and only a few Pt particles two layers in height are observed at 300 K. Therefore, for both Fe_3O_4(100) and (111) surfaces, Pt interacts strongly with magnetite, which leads, in essence, to Pt wetting of the oxide surface at room temperature.

For both systems, high-temperature annealing in UHV causes Pt sintering and the subsequent formation of well-faceted 3D nanoparticles with their edge at the interface running along the crystallographic direction of the oxide surface. These particles exhibit an octahedral shape on Fe_3O_4(111) but a cuboid shape on Fe_3O_4(001), following the epitaxial relationships between Pt and Fe_3O_4, that is, Pt(111)[110]//Fe_3O_4(111)[110][24] and Pt(001)[100]//Fe_3O_4(001)[100],[13] and thus resulting in particles that expose Pt(111) and Pt(001) top facets on Fe_3O_4(111) and Fe_3O_4(001), respectively. A notable difference is that Pt particles on Fe_3O_4(111) coalesce remarkably and form extended Pt islands,[3c,8] whereas Pt on Fe_3O_4(001) forms individual particles ≈5 nm in lateral size, at most. This finding could be indicative of the difference in adhesion energy and linked to the deformations on the two interfaces as a result of the mismatch between the two lattices. As another factor, our high-resolution electron microscopy studies of encapsulated Pt/Fe_3O_4(111) particles showed Fe enrichment of the interface between a Pt particle and an underlying support that results in more Pt–Fe bonds. As the Fe_3O_4(001) surface is initially terminated both by Fe and O atoms, it may well be that limited lateral growth of the Pt particles on Fe_3O_4(001) along the interface may be linked to the interface structure, which cannot be addressed with tools employed in the present study.

Conclusions

We studied the nucleation, growth, and thermal stability of Pt deposited on the ($\sqrt{2}\times\sqrt{2}$)R45°-reconstructed surface of Fe_3O_4(001) thin films. At low and medium coverages, Pt preferentially adsorbs monoatomically on the so-called "narrow" sites, that is, in the same manner as reported previously for Ag, Pd, and Au adatoms supported on a Fe_3O_4(001) single crystal. Vacuum annealing above 700 K leads to Pt sintering and concomitantly to reshaping (at ≈1000 K) into cuboid Pt nanoparticles with the edges oriented along the crystallographic directions of the Fe_3O_4(001) surface. In addition, high-temperature annealing suppresses CO adsorption on Pt, thus manifesting a SMSI effect by Pt encapsulation by the oxide support. The combined LEED, STM, and TPD results provide strong evidence for the encapsulating overlayer to be identified as FeO(111) as observed previously for a FeO monolayer film on a Pt(001) single crystal. The results are compared with those of the Pt/Fe_3O_4(111) system, which shows the encapsulation of (111)-oriented, hemispherical Pt nanoparticles by the FeO(111) layer. The comparison of the two systems suggests that the SMSI effect by encapsulation is insensitive to the surface structure of the oxide, although the latter strongly affects the particle morphology.

Experimental Section

The experiments were performed in an UHV chamber (base pressure 2×10^{-10} mbar) equipped with LEED and Auger electron spectrometers (from Specs), STM (Omicron), and a differentially pumped quadrupole mass spectrometer (QMS, Hiden 201) for TPD measurements. The Pt(001) crystal (99.95%, from MaTeck) was mounted on the Omicron sample holder and could be heated by electron bombardment from the backside of the crystal by using a tungsten filament. The temperature was measured by using a chromel-alumel thermocouple spot-welded to the edge of the crystal. The crystal temperature and the heating rate were controlled precisely by using a feedback system.

The Fe_3O_4(001) films were grown on a Pt(001) substrate as described in detail in Ref. [17]. Briefly, ≈3 nm Fe was evaporated onto the clean, hex-reconstructed Pt(001) surface at 300 K as a buffer layer, and subsequently 3 nm Fe was deposited with an O_2 background pressure of 5×10^{-6} mbar at 300 K. The sample was then UHV-annealed at 1020 K for 10 min. The quality of the prepared films was inspected each time by STM. Before Pt deposition, the Fe_3O_4(001) film was flashed to 600 K to desorb adventitious adsorbates.

Fe and Pt (both 99.95%, Goodfellow) were deposited by using commercial e-beam assisted evaporators (Focus EFM3). During Pt deposition, the sample was biased with a retarding potential to prevent metal ions from accelerating towards the sample. The STM images were obtained at 300 K with commercial Pt-Ir tips (LOT Oriel GmbH).

Acknowledgements

The work was supported by Fonds der Chemischen Industrie and German Science Foundation through Cluster of Excellence UNICAT administered by TU Berlin, and SFB 1109 administered by HU Berlin. The authors acknowledge COST Action CM1104.

Keywords: iron · platinum · supported catalysts · surface analysis · thin films

[1] S. J. Tauster, *Acc. Chem. Res.* **1987**, *20*, 389–394.

[2] a) J. Liu, *ChemCatChem* **2011**, *3*, 934–948; b) S. Penner, D. Wang, D. S. Su, G. Rupprechter, R. Podloucky, R. Schlögl, K. Hayek, *Surf. Sci.* **2003**, *532–535*, 276–280; c) S. Bernal, J. J. Calvino, M. A. Cauqui, J. M. Gatica, C. Larese, J. A. Pérez Omil, J. M. Pintado, *Catal. Today* **1999**, *50*, 175–206.

[3] a) O. Dulub, W. Hebenstreit, U. Diebold, *Phys. Rev. Lett.* **2000**, *84*, 3646–3649; b) Z. H. Qin, M. Lewandowski, Y. N. Sun, S. Shaikhutdinov, H. J. Freund, *J. Phys. Chem. C* **2008**, *112*, 10209–10213; c) Z. H. Qin, M. Lewandowski, Y. N. Sun, S. Shaikhutdinov, H. J. Freund, *J. Phys. Condens. Matter* **2009**, *21*, 134019; d) M. Bowker, P. Stone, P. Morrall, R. Smith, R. Bennett, N. Perkins, R. Kvon, C. Pang, E. Fourre, M. Hall, *J. Catal.* **2005**, *234*, 172–181.

[4] T. Suzuki, R. Souda, *Surf. Sci.* **2000**, *448*, 33–39.

[5] M. G. Willinger, W. Zhang, O. Bondarchuk, S. Shaikhutdinov, H.-J. Freund, R. Schlögl, *Angew. Chem. Int. Ed.* **2014**, *53*, 5998–6001; *Angew. Chem.* **2014**, *126*, 6108–6112.

[6] a) C. Kuhrs, Y. Arita, W. Weiss, W. Ranke, R. Schlögl, *Top. Catal.* **2000**, *14*, 111–123; b) Y. Joseph, W. Ranke, W. Weiss, *J. Phys. Chem. B* **2000**, *104*, 3224–3236; c) S. K. Shaikhutdinov, W. Weiss, R. Schlögl, *Appl. Surf. Sci.* **2000**, *161*, 497–507; d) W. Weiss, W. Ranke, *Prog. Surf. Sci.* **2002**, *70*, 1–151; e) R. S. Cutting, C. A. Muryn, G. Thornton, D. J. Vaughan, *Geochim. Cosmochim. Acta* **2006**, *70*, 3593–3612.

[7] a) R. Meyer, S. K. Shaikhutdinov, H. J. Freund, *Z. Phys. Chem. (Muenchen Ger.)* **2004**, *218*, 905; b) S. K. Shaikhutdinov, R. Meyer, M. Naschitzki, M. Bäumer, H. J. Freund, *Catal. Lett.* **2003**, *86*, 211–219.

[8] M. Lewandowski, Y. N. Sun, Z. H. Qin, S. Shaikhutdinov, H. J. Freund, *Appl. Catal. A* **2011**, *391*, 407–410.

[9] a) T. Kendelewicz, P. Liu, C. S. Doyle, G. E. Brown Jr., E. J. Nelson, S. A. Chambers, *Surf. Sci.* **2000**, *453*, 32–46; b) G. S. Parkinson, Z. Novotný, P. Jacobson, M. Schmid, U. Diebold, *J. Am. Chem. Soc.* **2011**, *133*, 12650–12655.

[10] a) Z. Novotný, G. Argentero, Z. Wang, M. Schmid, U. Diebold, G. S. Parkinson, *Phys. Rev. Lett.* **2012**, *108*, 216103; b) N. Spiridis, E. Madej, J. Korecki, *J. Phys. Chem. C* **2014**, *118*, 2011–2017; c) K. Jordan, S. Murphy, I. V. Shvets, *Surf. Sci.* **2006**, *600*, 5150–5157.

[11] G. S. Parkinson, Z. Novotny, G. Argentero, M. Schmid, J. Pavelec, R. Kosak, P. Blaha, U. Diebold, *Nat. Mater.* **2013**, *12*, 724–728.

[12] R. Bliem, R. Kosak, L. Perneczky, Z. Novotny, O. Gamba, D. Fobes, Z. Mao, M. Schmid, P. Blaha, U. Diebold, G. S. Parkinson, *ACS Nano* **2014**, *8*, 7531–7537.

[13] C. Gatel, E. Snoeck, *Surf. Sci.* **2006**, *600*, 2650–2662.

[14] a) A. Sala, H. Marchetto, Z. H. Qin, S. Shaikhutdinov, T. Schmidt, H. J. Freund, *Phys. Rev. B* **2012**, *86*, 155430; b) A. R. Lennie, N. G. Condon, F. M. Leibsle, P. W. Murray, G. Thornton, D. J. Vaughan, *Phys. Rev. B* **1996**, *53*, 10244–10253.

[15] a) R. Pentcheva, F. Wendler, H. L. Meyerheim, W. Moritz, N. Jedrecy, M. Scheffler, *Phys. Rev. Lett.* **2005**, *94*, 126101; b) Z. Łodziana, *Phys. Rev. Lett.* **2007**, *99*, 206402.

[16] R. Bliem, E. McDermott, P. Ferstl, M. Setvin, O. Gamba, J. Pavelec, M. A. Schneider, M. Schmid, U. Diebold, P. Blaha, L. Hammer, G. S. Parkinson, *Science* **2014**, *346*, 1215–1218.

[17] E. M. Davis, K. Zhang, Y. Cui, H. Kuhlenbeck, S. Shaikhutdinov, H.-J. Freund, *Surf. Sci.* **2015**, *636*, 42–46.

[18] G. S. Parkinson, Z. Novotný, P. Jacobson, M. Schmid, U. Diebold, *Surf. Sci.* **2011**, *605*, L42–L45.

[19] R. W. McCabe, L. D. Schmidt, *Surf. Sci.* **1977**, *66*, 101–124.

[20] Y. N. Sun, Z. H. Qin, M. Lewandowski, S. Shaikhutdinov, H. J. Freund, *Surf. Sci.* **2009**, *603*, 3099–3103.

[21] a) S. Shaikhutdinov, M. Ritter, W. Weiss, *Phys. Rev. B* **2000**, *62*, 7535–7541; b) G. H. Vurens, V. Maurice, M. Salmeron, G. A. Somorjai, *Surf. Sci.* **1992**, *268*, 170–178; c) M. Ritter, H. Over, W. Weiss, *Surf. Sci.* **1997**, *371*, 245–254.

[22] a) C. Lemire, R. Meyer, V. E. Henrich, S. Shaikhutdinov, H. J. Freund, *Surf. Sci.* **2004**, *572*, 103–114; b) S. Shaikhutdinov, W. Weiss, *J. Mol. Catal. A* **2000**, *158*, 129–133.

[23] X. Yu, X. Tian, S. Wang, *Surf. Sci.* **2014**, *628*, 141–147.

[24] C. Gatel, E. Snoeck, *Surf. Sci.* **2007**, *601*, 1031–1039.

Received: March 27, 2015